THE JOURNAL OF PHYSICAL CHEMISTRY B

Article

pubs.acs.org/JPCB

Exploring Electrochemical Windows of Room-Temperature Ionic Liquids: A Computational Study

Yong-Hui Tian,[†] George S. Goff,[‡] Wolfgang H. Runde,[‡] and Enrique R. Batista*[,†]

[†]Theoretical Division, Los Alamos National Laboratory, Los Alamos, New Mexico 87545, United States

[‡]Chemistry Division, Los Alamos National Laboratory, Los Alamos, New Mexico 87545, United States

Supporting Information

ABSTRACT: Room-temperature ionic liquids (RTILs) are regarded as green solvents due to their low volatility, low flammability, and thermal stability. RTILs exhibit wide electrochemical windows, making them prime candidates as media for electrochemically driven reactions such as electro-catalysis and electro-plating for separations applications. Therefore, understanding the factors determining edges of the electrochemical window, the electrochemical stability of the RTILs, and the degradation products is crucial to improve the efficiency and applicability of these systems. We present here computational investigations of the electrochemical properties of a variety of RTILs covering a wide range of electrochemical windows. We proposed four different approaches with different degrees of approximation and computational cost from gas-phase calculations to full explicit solvation models. It was found that, whereas the simplest model has significant flaws in accuracy, implicit and explicit solvent models can be used to reliably predict experimental data. The general trend of electrochemical windows of the RTILs studied is well reproduced, showing that it increases in the order of imidazolium < ammonium < pyrrolidinium < phosphonium giving confidence to the methodology presented to use it in screening studies of ionic liquids.

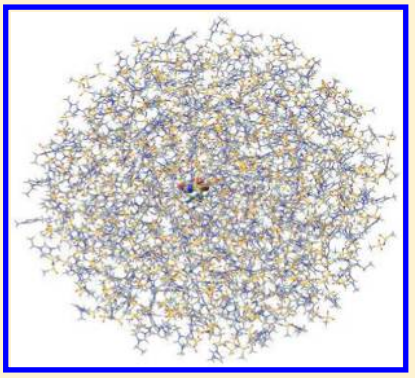

1. INTRODUCTION

Room temperature ionic liquids (RTILs) are organic salts that are typically in molten states below 100 °C. RTILs have attracted considerable attention due to their unique physiochemical properties such as negligible vapor pressure, high thermal stability, low flammability, and tunability of the properties by functionalizing the ion structures. Due to those advantages, RTILs are considered environmentally friendly solvents, and are attractive substitutes for conventional organic solvents, in particular for polar species and enzymes.[1] Another notable property of RTILs is their intrinsic electrical conductivity, making them useful as solvent in electrochemical systems without the need for supporting electrolytes. In recent years, RTILs have found applications in a variety of electrochemical processes such as lithium ion batteries,[2] fuel cells,[3] solar cells,[4] and electro-depositions.[5]

From the point view of practical electrochemical operations, the electrochemical stability of electrolytic media is one of the most important factors determining the utility and performance of electrochemical processes or devices. For instance, in energy storage and electro-deposition systems, the electrolyte should remain inert upon the application of voltage. The electrochemical stability of the ionic liquid is characterized by the electrochemical window (ECW). The electrochemical window is defined as the potential interval between the cathodic and anodic potential limits, at which reduction and oxidation reactions of electrolytes occur on the electrodes. Experimentally, a linear sweep or cyclic voltammetry (CV) is commonly used to measure electrochemical windows, in which the cathodic or anodic limits are determined as the potentials at where the current density in the cell reaches a standard value, typically 1.0 mA/cm^3. Many RTILs have been shown to exhibit electrochemical windows over 5 V, which is significantly wider than those of aqueous or organic electrolytic media.[6] Owing to this remarkable feature in combination with the aforementioned advantages, RTILs have been considered as promising electrolytic media and intensely developed for various electrochemical devices. At the moment, it is estimated that over 1000 RTILs are available, although not fully characterized, and on the order of 10^{18} possible ionic liquids should be feasible.[7]

The electrochemical windows have been experimentally investigated for RTILs composed of a variety of cation and anion couples. The most common cations of ionic liquids are characteristic of large size, including imidazolium, pyrrolidinium, quaternary ammonium, or phosphonium, the structures of which are depicted in Figure 1. For the major RTILs used for electrochemical processes, it is generally suggested that the cation stability increases in the order of imidazolium[8] < quaternary ammonium (QA)[9] < pyrrolidinium (PYR)[10] < quaternary phosphonium(QP).[11] It is noted that the electrochemical redox processes of RTILs are usually irreversible and the measured electrochemical windows are not strictly electrochemically defined. Moreover, the measured potential limits are highly dependent on experimental conditions such as

Received: April 23, 2012
Revised: August 31, 2012
Published: September 4, 2012

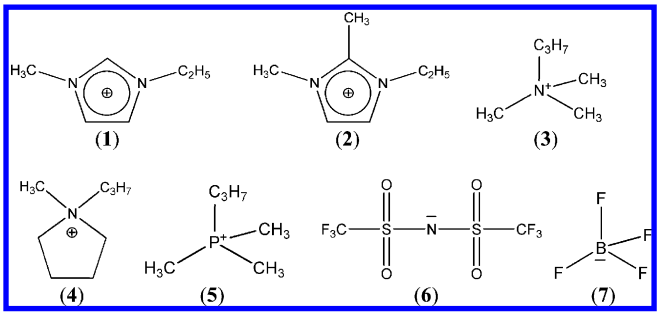

Figure 1. The structures of cations and anions used for calculations: **1**, 1-ethyl-3-methylimidazolium (C_2MIM); **2**, 1-ethyl-2-methyl-3-methylimidazolium (C_2MMIM); **3**, trimethylpropylammonium (N_{1113}); **4**, *N*,*N*-propylmethylpyrrolidinium (PYR_{13}); **5**, trimethylpropylphosphonium (P_{1113}); **6**, bis(trifluoro-methylsulfonyl)-imide (Tf_2N); **7**, tetrafluoroborate.

impurities and the type of electrode used. As a result, one finds variations in the electrochemical data in the literature even for the same RTILs.

The electrochemical redox reactions of RTILs have also been experimentally investigated in the literature. Generally, it is assumed that the observed cathodic and anodic potential limits are associated with the reduction of cations and oxidation of anions, respectively.[12] For the case of imidalolium-based RTILs, it was hypothesized that the reduction of cations is related to the H(2) deprotonation.[8] This hypothesis is based on the observation of stable carbines when the imidazolium cations are deprotonated with strong bases.[13] For quaternary ammonium, it is believed that one of the carbon nitrogen bonds breaks apart upon one electron reduction, forming an amine molecule and an alkyl radical.[14]

Theoretical works on the electrochemical stability of RTILs are rare in the literature. In a previous theoretical report, the electrochemical windows were calculated by using the polarizable continuum model at the Hartree−Fock (HF) level.[15] The calculated results are in general agreement with experiments for several RTILs. However, in those calculations, a dialectic constant of 69 was used, which is significantly larger than the experimentally suggested value of 12 for those kinds of RTILs. Moreover, in those calculations, the structures of ionic species kept their integrity upon electrochemical redox reactions, which is in contradiction with experimental evidence that the anions or cations may decompose in the electrochemical processes. More details about this will be discussed later in our paper. Another aspect of those calculations is that all the calculations were based on the HF level, which might be insufficient for electron affinity or ionization energy calculations. A recent study has carried out calculations by using both cluster models (with a reaction field for the medium) and periodic DFT methods in combination with classic molecular dynamics simulations to equilibrate the system configurations.[16] According to this report, the cluster model overestimates the ECWs, while the predictions by the extended system underestimated them. It is noticed in this study that the energetics were calculated without taking account of the inner sphere or outer sphere relaxation upon redox reactions. The ECWs would be further underestimated by the periodic DFT calculations, if reorganization energies were accounted for. Furthermore, some important chemical reactions of decomposition may have been missed in such vertical calculations. A computational investigation has been carried out to correlate the substitution effect and the gas-phase electron affinities and ionization energies of RTILs.[17]

In this context, the present work addresses the following issues: (1) Find reliable and efficient methods for modeling the electrochemical windows of the commonly used RTILs. With such methods, we hope to, in future work, screen for suitable candidate RTILs for certain electrochemical purposes among the huge number of RTILs developed so far, and to make predictions of the electrochemical properties for new RTIL systems. (2) To accurately predict the electrochemical windows, it is essential to understand the electrochemical reactions at cathodic and anodic limits for a given RTIL. Therefore, one of the focuses of this work is to computationally find the most favorable electrochemical redox processes among the possible reactions. (3) Explore the factors dominating the electrochemical windows. It can be envisioned that the electrochemical stability of RTILs is related to the intrinsic properties of the ionic species as well as solvation effects. We will carry out detailed investigations of these two effects for specific ionic systems.

2. COMPUTATIONAL METHODOLOGIES

2.1. Selected RTILs for Modeling. The structures of RTILs involved in this investigation are shown in Figure 1. In combination with the Tf_2N^- and BF_4^- anions, a variety of cations were used, including imidazolium, quaternary ammonium (QA), pyrrolidinium (PYR), and quaternary phosphonium (QP) covering a relatively wide range of electrochemical windows according to experiments. Imidazolium is an aromatic cation, in which the positive charge is delocalized on the ring. On the other hand, for QA, PYR, and QP, the charges are relatively localized. The structural diversity of these cations is advantageous to examine the applicability of our computational methods to general RTILs, and it is helpful as well to explore the factors affecting the electrochemical stability of cations.

2.2. Calculations of Cathodic/Anodic Potential Limits and Electrochemical Windows. In this study, the calculated cathodic or anodic limits correspond to the potentials at the equilibrium state for a given RTIL system. That means the estimated potentials refer to the rest situations, i.e., to the potentials in the absence of electrical current passing the electrolytic systems. For this reason, the calculated potentials might deviate from the experimental values that include overpotentials. However, besides accuracy, we are more concerned with predicting the trend of electrochemical windows for a variety of RTILs already developed, and for those to be synthesized.

For the calculations of cathodic or anodic potential limits, the corresponding electrochemical reactions need to be clarified. Herein, we assume that cations are reduced and anions are oxidized in the electrochemical redox reactions, the reason for which will be justified below. For equilibrated systems, the electrode potential is estimated by the Nernst equation:

$$V_{ox} = \Delta G^{ox}/nF = (G(A) - (G(A^-))/nF \quad (1)$$

$$V_{red} = \Delta G^{red}/nF = (G(C) - G(C^+))/nF \quad (2)$$

where V_{ox} and V_{red} refer to oxidization and reduction potentials corresponding to certain redox reactions, n is the number of electrons involved in the corresponding redox processes, F is the Faraday constant, ΔG^{ox} and ΔG^{red} are the respective free energy changes associated with the redox couples C^+/C and A^-/A involved in the corresponding redox reactions, and C^+

dx.doi.org/10.1021/jp303915c | J. Phys. Chem. B 2012, 116, 11943−11952

and C are general designations of the cations and their reduced products, respectively. A^+ and A mean anions and the corresponding oxidized products, respectively. In a reductive or oxidative decomposition reaction, the reduction product C or oxidation product A may include several species, as will be shown by some of the reactions in section 4. In point of energetics, the anodic potential limit is determined by the reaction in which the reactive species gain the least amount of energy during the oxidation process. On the other hand, the cathodic limit is related to the reaction where the reacting species lose the most energy during the reduction processes. Correspondingly, as shown in eqs 3 and 4, the cathodic limit or reduction stability of a RTIL system is defined as the minimum of the reduction potentials among the possible reduction reactions, while the anodic limit or oxidation stability is determined by the minimum of all possible oxidation potentials and their corresponding oxidation reactions.[16]

$$V_A = \min(V_{ox,1}, V_{ox,2}, V_{ox,3}, ...) \quad (3)$$

$$V_C = \min(V_{red,1}, V_{red,2}, V_{red,3}, ...) \quad (4)$$

The electrochemical window (ECW) is defined as

$$ECW = V_A + V_C \quad (5)$$

In this work, we assume that the anodic limit is set by oxidation of anions, and the cathodic limit is set by reductions of cations for most of the ionic systems. On the other hand, for some specific RTILs, a recent report suggests that some cation species are prone to be oxidized before the oxidation of anions.[16] Likewise, it is possible that some anion species are more preferable to be reduced than the cations. Accordingly, the cathodic limits might be determined by reduction of anions, and anodic limits might be determined by oxidation of cations. For those systems, we also examined these possibilities, as will be shown for $[C_2MIM]^+[BF_4]^-$ and $[PYR_{1113}]^+[Tf_2N]^-$.

2.3. Methods to Calculate the Free Energy Changes. To calculate the free energy changes upon redox reactions (ΔG^{ox} and ΔG^{red} as shown in eqs 1 and 2), four theory levels were used, including DFT calculations in gas phase, polarizable continuum model (PCM), thermodynamic cycles (TDC), and ONIOM method.

2.3.a. Gas Phase Single-Molecule Calculations. In the simplest level, the free energy, G, of an individual ion in the gas phase was routinely calculated by the first principle method as discussed in the following sections. By this method, the free energy was calculated as follows:

$$G = H - TS = E_0 + E_{ZPE} + E_{therm} + k_B T - TS \quad (6)$$

where H is enthalpy, T is temperature, S is entropy, E_0 is electronic energy, E_{ZPE} is zero point energy, E_{therm} is the thermal correction to the internal energy, and k_B is Boltzmann constant. The terms of E_{therm} and S are associated with the partition functions contributed by translations, rotations, vibrations, and electronic motions. The method to calculate thermodynamics is based on the textbook formulations[18] as implemented in the Gaussian 09 program.[19] With the free energies of reactants and products, the corresponding reaction free energy change can be obtained by eqs 1 and 2.

2.3.b. Single-Molecule Calculations with Reaction Field. In the second method to calculate free energy changes, the solvation effects were implicitly accounted for by using a reaction field via a polarizable continuum model (PCM). Specifically, the universal solvation model,[20] SMD developed by Truhlar et al., was used. In this model, the solvent was treated as a continuous medium with the dielectric constant of the ionic liquid. An individual ion was embedded in solvents, and a cavity was created, the surface of which was polarized to mimic the polarization of the solute species. The respective terms to define free energies are similar to those in the gas phase calculations shown in eq 6 except that there are extra terms to account for the free energy of the cavity. In PCM calculations, dichloromethane (DCE) was used as a solvation medium,[21] which has a dielectric constant of 10.36 close to that of 12 for typical RTILs.[22] All of the molecules including reactants and products have been geometrically optimized, and energy calculations were based on the optimized geometries.

2.3.c. Single-Molecule Calculations Plus Thermodynamic Integration for Solvation Energy. Thermodynamic cycle (TDC) is another method we used to indirectly calculate free energy differences between reactant and products for each ion.[23] The TDCs are depicted in Figure 2a and b

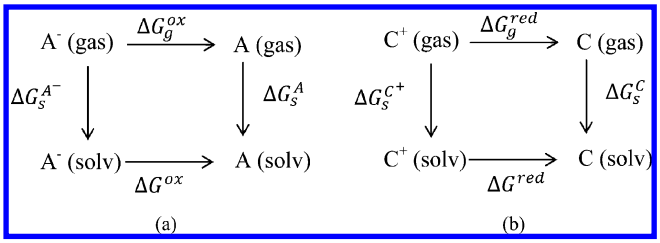

Figure 2. Thermodynamic cycles used to calculate free energy changes corresponding to the oxidation (a) and reduction reactions (b). See the text for the meaning of the labels.

corresponding to the oxidation of anions and reduction of cations, respectively. In this method, the calculation of free energy change is reduced to two parts, the reaction free energy in the gas phase (ΔG_g^{ox}, ΔG_g^{red}) and the solvation free energy of the reactive species (ΔG_s^{A-}, ΔG_s^{A}, ΔG_s^{C+}, ΔG_s^{C}). The reaction free energies in the gas phase can be calculated quantum mechanically, while the solvation free energies are estimated with thermodynamic integration or free energy perturbation technique by using classic molecular dynamic (MD) simulations. The calculation of the solvation free energy follows that described in ref 26, and a brief description of this methodology is given in section 2.4 for the benefit of the reader. The overall reaction free energies (ΔG^{ox}, ΔG^{red}) can be characterized by eqs 7 and 8.

$$\Delta G^{ox} = \Delta G_g^{ox} + (\Delta G_s^{A} - \Delta G_s^{A^-}) = \Delta G_g^{ox} + \Delta\Delta G_s^{A^-/A} \quad (7)$$

$$\Delta G^{red} = \Delta G_g^{red} + (\Delta G_s^{C} - \Delta G_s^{C^+}) = \Delta G_g^{red} + \Delta\Delta G_s^{C^+/C} \quad (8)$$

2.3.d. Quantum Mechanics/Molecular Mechanics Model for Solvation. The two-layer ONIOM method[24] was used to calculate the reaction free energy changes. In this method, the reactive species are treated by first principle, while the environment is described by molecular mechanics (MM). The total ONIOM energy can be written as

$$E_{ONIOM} = E^{real,MM} + E^{model,QM} - E^{model,MM}$$

dx.doi.org/10.1021/jp303915c | J. Phys. Chem. B 2012, 116, 11943−11952

where, according to the convention introduced by Morokuma, $E^{real,MM}$ is the calculated energy at the MM level for the real system containing all the atoms, $E^{model,QM}$ is the energy calculated at high level for the atoms in the QM region, and $E^{model,MM}$ corresponds to the energy calculated at the MM level for the QM atoms. The electrostatic embedding scheme was used to describe the electrostatic interactions between the MM region and QM region. In this scheme, the partial charges of the MM regions are incorporated into the quantum mechanic Hamiltonians, and the QM part is therefore polarized by the MM region atoms.

2.4. Calculating Solvation Free Energies by Classical MD Simulations. The solvation free energies (ΔG_s^{A-}, ΔG_s^{A}, ΔG_s^{C+}, ΔG_s^{C} in Figure 2) can be regarded as the free energy difference of an ion in gas phase and solvation. Whereas there exist a variety of methods in the literature to estimate the free energy difference of two states through classical MD simulation,[25] we adopted the Bennett ratio method[26] for the studies presented here.

In solvation free energy calculations, the solvent−solute interactions are decoupled in gas phase state Hamiltonians, while, for solvated states, the solvent−solute interactions are fully accounted for in the corresponding Hamiltonians. For the case of RTIL systems, the Hamiltonian perturbations between the gas phase state and solvated state are very strong due to the net charges on ionic species. Therefore, to improve the phase overlap problem, a number of intermediate states need to be added between the two target states. In these intermediate states, the solutes are partially solvated by using the following model Hamiltonians as a function of coupling parameter λ:

$$H(\lambda) = (1 - \lambda)H_C + H_{vdW} \tag{9}$$

where H_C designates solvent−solute Columbic interaction potentials and H_{vdW} is the potential only accounting for van de Waals (vdW) interactions. The solvent−solute Columbic interactions are gradually switched off by varying λ from 0 to 1, which corresponds to the fully solvated state and Coulombically decoupled state, respectively. In this work, the value of λ increases from 0 to 1 in increments of 0.05. The free energy difference for any two neighboring states is calculated by using the Bennett ratio acceptance method, and the solvation free energy is obtained by summing the energies of the neighboring states, as shown in eq 10.

$$\Delta G_{solv} = -\sum_{i=0}^{i=0.95} \Delta G_{solv}^{\lambda_{i\rightarrow i+0.05}} \tag{10}$$

It is noted that, in eq 9, only Columbic interactions are switched off in the decoupled states, and hence the calculated solvation free energies only account for the electrostatic contributions. According to a previous report, the vdW contributions to the solvation energies difference between reactants and products ($\Delta\Delta G_{solv}^{A^-/A}$ and $\Delta\Delta G_{solv}^{C^-/C}$ in eqs 7 and 8) are less than 1.0 kcal/mol;[27] therefore, the neglect of vdW contributions would not significantly affect the estimation of electrode potential limits and electrochemical windows.

3. COMPUTATIONAL DETAILS

All the first principle calculations were carried out by using the Gaussian 09 program.[19] The geometries were optimized with B2PLYP(D)[28] combined with the 6-311++G(2d,p) basis set. The convergence criteria of geometry optimization were set to the default values in Gaussian 09. In this double hybrid method developed by Grimme, exact HF exchange and an MP2-like correlation are combined into DFT calculations. An empirical term, D, is added to the B2PLYP calculations for dispersion correction.

All molecular dynamics (MD) simulations were performed with the GROMACS package.[29] The force field parameters developed by Lopes[30] were used for all of the RTILs involved in this study. The simulation boxes contain a total of 200 anion−cation pairs. All atoms were treated explicitly, and the simulations were carried out under periodic boundary conditions. The integration step size of 0.5 fs was used for all simulations. The nonbonded interactions were cut off at a radius of 16 Å. The long-range Coulomb interactions were calculated by the fast particle-mesh Ewald summation scheme. Prior to MD simulations, the structures were relaxed by minimizing the energies with the conjugate gradient method to remove the close contacts between ions. In the second step, the systems were gradually heated up to 600 K in 100 ps in NPT ensembles, and then equilibrated for 500 ps at 600 K for a thorough mixing. Subsequently, the systems were cooled down to 298 K during 100 ps followed by an equilibration process at 298 K for 1 ns. With the equilibrated configurations, the systems were sampled for 1 ns for each λ point to calculate solvation free energies.

The Gaussian 09 package was employed for ONIOM calculations. The structures used for ONIOM calculations were taken from pre-equilibrated configurations with MD simulations. Specifically, a total number of 600 ion pairs in a three-dimensional box were simulated following the same procedure as mentioned before. The ions within a sphere of radius about 35 Å were cut off from the equilibrated boxes. Subsequently, MD simulations were run to further equilibrate the spherically truncated structures by fixing the edge ions beyond 26 Å from the center and a central ion that will be treated by QM level in subsequent ONIOM cancelations. It is noted that, for each oxidation state of the ions, this MD procedure was repeated to allow solvation relaxation upon redox reactions. Then, for each oxidation state, 20 snapshots were taken every 10 ps from the corresponding equilibrated simulations for later ONIOM geometry optimization and energy calculations, and the 20 ONIOM energies were averaged for electrochemical window calculations. During the geometry optimization with ONIOM, the ions on the sphere edge were fixed and only the ions confined in the interior of the spheres were allowed to relax. This was done to avoid the edge effect and make the calculations consistent for the same kind of ions but with different oxidation states. The reactive parts (or QM region) were placed at the center of the sphere, and were treated at the B2PLYP(D)/6-31+G(dp) level for geometry optimization and at B2PLYP(D)/6-311++G(2d,p) for single point energy calculations. The thermodynamic corrections were based on the gas phase calculations of individual ions at their respective oxidation states. The MM regions were described by using the same force filed as for MD simulations. A sample ONIOM optimized structure is illustrated in Figure 3 for the $[C_2MIM]^+[Tf_2N]^-$ system, where a Tf_2N anion is centered in the sphere and treated at a high level of theory.

4. RESULTS AND DISCUSSION

This section is organized as follows. In subsections 4.1 and 4.2, the electrochemical windows of RTILs are discussed with respect to the type of cations distinguished by charge

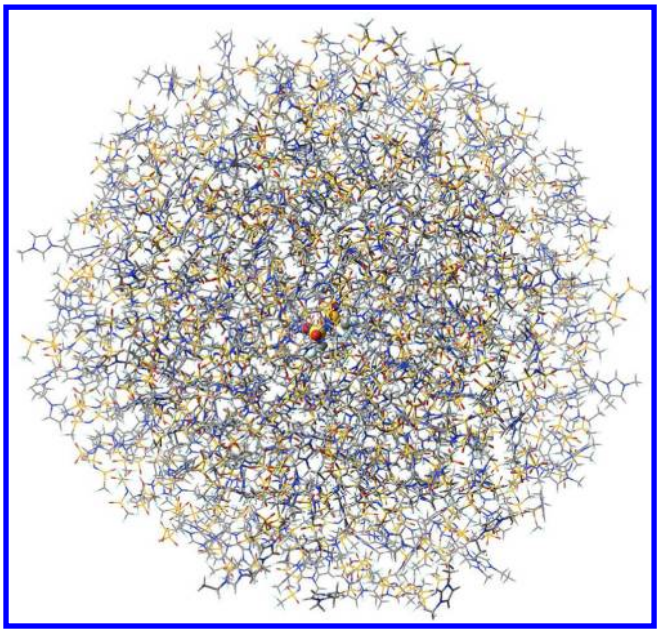

Figure 3. The ONIOM optimized structure of the $[C_2MIM]^+[Tf_2N]^-$ system. The central reactive part depicted in bold was treated at the B2PLYP(D) level, and the environment was described at the MM level.

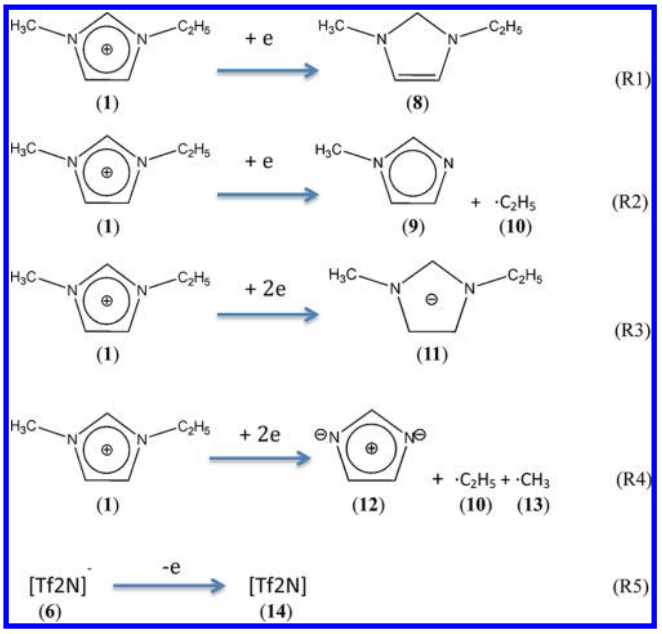

Figure 4. The redox reactions used to calculate reduction potentials. The other possible reactions were excluded due to the high energies of the corresponding reaction products according to the calculations.

delocalization or localization. The $[Tf_2N]^-$ anion was used in combination with all the cations covered in this study. To evaluate the validity of computational methods, another anionic species, $[BF_4]^-$, in combination with $[C_2MIM]^+$ was also examined, and the calculated redox potentials were reported in subsection 4.1. For each type of cations, only one RTIL system was calculated for performance evaluation by using all of the four computational methods including isolated ions in the gas phase, PCM, TDC, and ONIOM. In subsection 4.3, the trend of electrochemical windows was summarized in terms of the structures of cations.

4.1. Electrochemical Windows of Imidazolium-Based RTILs. In this section, the focus is placed on RTILs based on charge delocalized cations including $[C_2MIM]^+$ (**1**) and $[C_2MMIM]^+$ (**2**). To understand the electrochemical stability of RTILs, we first examined the possible redox reactions of cations and anions in ionic environments. Due to the electron π-conjugation character of imidazolium cations, the redox reactions are characterized by structural diversity of reduction products. Among those possibilities, we will find the most favorable reactions in the ionic environments, which determines the cathodic potential limits. The possible reduction reactions of imidazolium are listed in Figure 4. In reaction R1, the cation is one-electron-reduced to a neutral state, while, in R2, bond breaking occurs upon one-electron reduction, producing a closed shell neutral molecule and an alkyl radical. Reactions R3 and R4 correspond to two-electron reduction reactions with bond breaking occurring in the later process. Deprotonation reaction at the C2-position has been proposed in the literature.[8] Our calculations precluded this possibility due to the considerably high energy (the reduction state is 12.8 eV higher than the cation state according to the gas phase calculations) of the reduction product compared to the reactions listed in Figure 4. For the oxidation reaction of $[Tf_2N]^-$ anion, reaction R5 was used. Corresponding to the possible redox reactions, the calculated cathodic and anodic potentials are tabulated in Table 1. The more negative reduction potentials mean more stable reduction products, and accordingly, the corresponding reactions are more likely to occur.

In *vacuo* calculations, the solvation effect is not included, and the redox potentials are associated with the intrinsic properties of the reactive molecules. It is shown that reaction R2 is the most preferable reduction process for imidazolium cation in the gas phase. However, the corresponding electrochemical window according to eqs 3−5 is 0.84 V, which is significantly smaller than experimental values. This is not surprising, since the effect of solvent is missing in this simple model. Despite the considerable deviation from experiments, the gas phase calculations still show the intrinsic stabilities of the reduction products. For the one-electron reduction reactions (R1 and R2), the corresponding oxidized states are both neutral. However, reaction R2 is much more favorable over R1. This can be understood simply by counting the π-electrons on the five-member ring of the reduction products. In imidazolium cation (**1**), there are six π-electrons, and hence this molecule is aromatically stabilized according to the $4n + 2$ rule. In the reduction product (**8**), the sp^2 carbon at the C2-position is hybridized to sp^3 carbon and the reduction product is relatively destabilized due to broken π-conjugation and electron crowdedness on the small ring. However, for reaction R2 and corresponding product (**9**), the extra electron upon reduction can be accepted by the one-electron occupied sp^2 orbital on the nitrogen atom, where the bond scission occurs. Consequently, there are still six π-electrons in the molecules (**9**) that are stabilized by aromaticity. The relative stability for the reduced products (**11** and **12**) from reactions R3 and R4 can be understood from the same reasoning. Upon the two-electron reduction (R4), the two carbon−nitrogen bonds break, and the two extra electrons are localized on the two one-electron occupied sp^2 orbitals of the two nitrogen atoms in product **12**, thus remaining aromaticity. In contrast, in reaction R3 and molecule **11**, there are eight π-electrons on the ring that destabilize the structure due to strong Coulomb repulsions.

dx.doi.org/10.1021/jp303915c | J. Phys. Chem. B 2012, 116, 11943−11952

Table 1. The Calculated Potentials (in V) of $[C_2MIM]^+[Tf_2N]^-$ Corresponding to the Redox Reactions in Figure 4[a]

	$V(R5)_{ox}$	$V(R1)_{red}$	$V(R2)_{red}$	$V(R3)_{red}$	$V(R4)_{red}$	ECW	Exp.
vacuo	5.40	−3.82	−4.56	−1.75	−2.09	0.84	4.1[31]
PCM	7.00	−1.85	−2.72	−1.75	−2.17	4.28	4.5[8,9c]
TDC	7.02	−1.68	−2.55			4.47	
ONIOM	7.55	−2.39	−2.94			4.61	

[a]The most negative reduction potentials were used to calculate the electrochemical windows (ECW) according to eqs 3−5 (an example was given in the Supporting Information to show the details of the ECW calculations).

The above justifications can be verified by inspecting the natural bonding orbitals of the respective reduction products, as illustrated in Figure 5. From the localized orbitals, it is clearly seen that the nitrogen lone pair orbitals are doubly occupied for the reduced products **9** and **12**. On the other hand, the molecular ring is bent at the C2-position upon one-electron reduction in reaction R1.

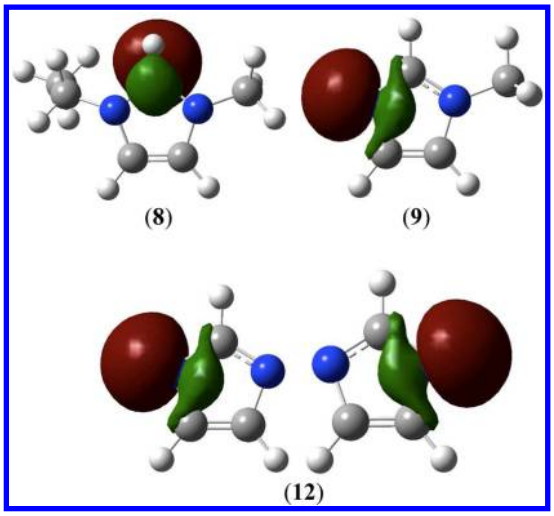

Figure 5. Natural bonding orbitals showing the localization of the extra electron on the ring molecules upon reduction reactions of imidazolium cations. In **8**, the orbital is singly occupied, and in **9** and **12**, all the orbitals are doubly occupied.

When the solvation effect is included in the calculations by using the PCM model, the calculated results are dramatically improved compared to the gas phase calculations. The calculated electrochemical windows are in good agreement with experimental values, as shown in Table 1. The PCM calculations also predict that the reduction reaction R2 is the most preferable one among the possible processes. The calculated solvation free energies are listed in Table 2. It is noted that, for the charged species, the solvation free energies (ΔG) are proportional to q^2/r (q is the charge and r is the radius of the cavity) according to the Born model, while, for neutral species, $\Delta G \propto \mu^2/r^3$ (μ, dipole moment). Accordingly, the charged species usually exhibit much stronger solvation than the neutral species, which is in line with the calculations shown in Table 2. The strong solvation effect of the cationic or anionic species makes them resistant to reduction or oxidation. Accordingly, the calculated electrochemical windows are wider than those calculated in gas phases. Another observation from PCM calculations is that the reduced species **9** and **10** exhibit slightly stronger solvation stability than the reduction product **8**, which causes the reduction R2 more favorable over R1.

Notably, in a previous report,[16] it was demonstrated that PCM calculations considerably overestimated the electrochemical windows of imidazolium-based RTILs. Nonetheless, our PCM calculations agree well with experiments. The major reason for this difference between our approach and ref 16 might be from the redox reactions used to calculate the potential limits and ECWs. We used the most favorable reduction reaction corresponding to the one-electron process R2 shown in Figure 4. However, in the previous report, the reduction potential limits were estimated on the basis of the one-electron reduction reaction R1 that is unfavorable compared to reaction R2 as aforementioned. This led to approximately 1 eV overestimation of the electrochemical windows.

In addition to the PCM method, the electrochemical windows were also calculated with the TDC and ONIOM methods, both of which comprise solvation effects. To save computational cost, the TDC and ONIOM calculations were carried out only for the one-electron reduction reactions (R2) that show priority over the other processes, as suggested by the PCM calculations. As shown in Table 1, the calculated electrochemical windows by the TDC and ONIOM methods agree well with the PCM model and experimental values. This is an interesting result because the molecular mechanics model for the explicit solvent does not include electrical polarizabilities. We think that, because of the ionic nature of the solvent, the induced polarization could stem from relative displacement of anions and cations from the chemical species under study, in response to the charge state. Consequently, we think that this validates the PCM model to be used as a computationally efficient method to predict the electrochemical windows of imidazolium based ionic liquids, reducing significantly the computational cost of these studies. Another

Table 2. Solvation Free Energies (in eV) Corresponding to the Redox Reactions R1−R5 Described in Figure 4[a]

	$\Delta G(\mathbf{1})_s$	$\Delta G(\mathbf{8})_s$	$\Delta\Delta G_s^{R1}$	$\Delta G(\mathbf{9,10})_s$[b]	$\Delta\Delta G_s^{R2}$	$\Delta G(\mathbf{6})_s$	$\Delta G(\mathbf{14})_s$	$\Delta\Delta G_s^{R5}$
PCM	−2.38	−0.39	2.01	−0.53	1.85	−1.59	0.01	1.60
TDC	−2.28	−0.14	2.14	−0.27	2.01	−1.72	−0.10	1.62
	$\Delta G(\mathbf{1})_s$	$\Delta G(\mathbf{11})_s$	$\Delta\Delta G_s^{R3}$	$\Delta G(\mathbf{10,12,13})_s$[b]		$\Delta\Delta G_s^{R4}$		
PCM	−2.38	−2.43	−0.05	−2.52		−0.14		

[a]$\Delta\Delta G_s^{R1-R5}$ were calculated as the solvation free energy differences of the products and reactants as described in eqs 7 and 8. For reactions R3 and R4, only PCM calculations are reported. [b]Summation of the solvation free energies corresponding to all of the reduction product species.

Table 3. The Calculated Potentials (in V) Corresponding to the Redox Reactions in Figure 1S (Supporting Information)[a]

	$V(R5)_{ox}$	$V(R1)_{red}$	$V(R2)_{red}$	$V(R3)_{red}$	$V(R4)_{red}$	ECW	Exp.
vacuo	5.40	−3.60	−4.41	−1.67	−1.98	0.99	4.4,[33] 4.7[8]
PCM	7.00	−1.72	−2.65	−1.67	−2.08	4.35	

[a]The most negative reduction potentials were used to calculate the electrochemical windows according to eqs 3−5.

observation from Table 2 is that the PCM method predicts slightly stronger solvation than does the TDC method. It is known that, in the PCM model, the reactive molecules are polarizable by the continuum media, while the TDC model we used is silent on polarizations. Therefore, the polarizable force field might be needed to improve the TDC calculations of solvation free energies involved in ionic liquids. Actually, the importance of polarizations has been emphasized in several studies on dynamical properties of RTILs.[32] For ONIOM calculations, the active molecules are polarizable by comprising the MM point charges in the Hamiltonians of the QM regions, and hence, the solvation effect is covered at this level. However, it is difficult to separate the solvation free energies from ONIOM calculations.

The following calculations were carried out at the PCM level of theory for other imidazolium-based RTILs that have a similar structure as $[C_2MIM]^+$ (**1**). This system is composed of $[Tf_2N]^-$ anions and $[C_2MMIM]^+$ (**2**), the structure of which is shown in Figure 1. RTILs based on $[C_2MMIM]^+$ are of interest, for it is experimentally observed that methyl substitution on the C2 position gives rise to stronger cathodic stability of the cations.[8] In the calculations for $[C_2MMIM]^+[Tf_2N]^-$, similar redox reactions were used as for the $[C_2MIM][Tf_2N]$ system as described in Figure 4. The reaction diagrams are shown in the Supporting Information, Figure 1S. The calculated potential limits are listed in Table 3. Here, the one-electron reduction with the involvement of bond scission is still the most favorable process. Notably, the calculations predict a slightly wider electron chemical window compared to the $[C_2MIM]^+[Tf_2N]^-$ system, which is consistent with trend observed in experiments. On the basis of the hypothesized mechanism of hydrogen abstraction upon the reduction for $[C_2MIM]^+[Tf_2N]^-$, it has been previously supposed that methyl substituted imidazolium would be more reduction resistant.[8] However, on the basis of reduction reaction R2, our calculations suggest that the wider electrochemical windows for $[C_2MMIM]^+[Tf_2N]^-$ might be due to the strong steric repulsions between the methyl group and the long pair in the one-electron reduction product, which is absent in the reduction product of $[C_2MIM]^+$. Therefore, $[C_2MIM]^+$ is easier to be reduced than $[C_2MMIM]^+$.

The $[C_2MIM]^+[BF4]^-$ system was also investigated. The possible cathodic reduction reactions related to cations are the same as those aforementioned. Here the most favorable process R2 was taken for ECW calculations. However, for oxidation reactions, there are a number of possible processes as depicted in Figure 6. In reaction R6, The molecule keeps integrity upon reduction, but the symmetry was lifted from *Td* to *C2v*. In reaction R7, bond abscission occurs. In R8, a fluorine transfer process was computationally observed. In this process, we assumed a one-step process, i.e., the reduction reaction accompanied by fluorine atom transfer. The structure of product **18** is shown in Figure 7. In a previous computational study of $[C_4MIM]^+[BF_4]^-$ systems,[16] the anodic potential limit was set by the oxidation of imidazolium cations. We also examined this possible process, as shown by R9 in Figure 6.

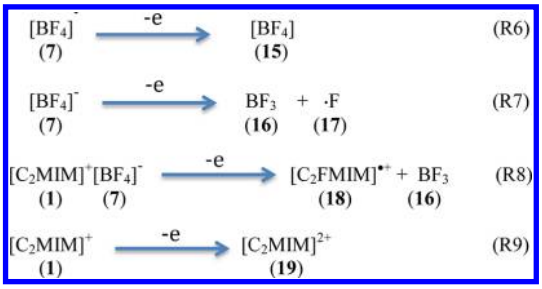

Figure 6. The oxidation reactions identified by calculations.

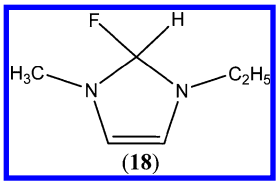

Figure 7. The chemical structure of molecule **18**.

The calculated potential limits and ECWs are summarized in Table 4. In *vacuo* model, R8 is the most viable path. However, the calculated ECW deviates from experimental value. Upon incorporation of solvent effect, the R8 reaction is still the most favorable, and the calculated ECW agree well with experiment. Our prediction is different from the previous computational report where the R9 was suggested to be the oxidation potential limit process. Further experimental evidence is needed to resolve this issue.

4.2. Electrochemical Windows of RTILs Based on Quaternary Ammonium (QA) and Quaternary Phosphonium (QP). All of the cations involved in this subdivision are characterized by charge localization. The electrochemical windows calculated at a variety of levels are shown in Table 5 for the $[N_{1113}]^+[Tf_2N]^-$ system, and the corresponding redox reactions are shown in Figure 8. The same oxidation process was used for $[Tf_2N]^-$ anions, as described in Figure 4. For $[N_{1113}]^+$ cations, two possible one-electron reduction reactions are identified by our calculations. In reaction R10, the molecular cation keeps its integrity upon reduction, while, in reaction R11, one of the carbon−nitrogen bonds breaks. The gas phase calculations show that the bond breaking reaction R11 is intrinsically more preferable over the reaction R10. In comparison with $[C_2MIM]^+$, $[N_{1113}]^+$ cations exhibit weaker reduction stability in the gas phase. This might be due to the different electronic structures of the two kinds of cations, with the nitrogen atoms being sp^2 and sp^3 hybridized for $[C_2MIM]^+$ and $[N_{1113}]^+$, respectively. Expectedly, the calculated electrochemical window in the gas phase deviates far from the experimental values.

When the solvation effect is recovered by using the PCM, TDC, and ONIOM methods, the predicted electrochemical windows approach the experiment measurements. The computationally efficient PCM model exhibits comparable accuracy with the TDC and ONIOM method. Given the fact that the electrochemical windows reported in the literature vary

Table 4. The Calculated Potentials (in V) Corresponding to the Redox Reactions in Figure 6[a]

	$V(R6)_{ox}$	$V(R7)_{ox}$	$V(R8)_{ox}$	$V(R9)_{ox}$	$V(R2)_{red}$	ECW	Exp.
vacuo	7.12	6.43	4.98	13.74	−4.56	0.42	4.3[6a,12b]
PCM	9.43	8.68	7.19	7.59	−2.72	4.47	

[a]The smallest oxidation potentials were used to calculate the electrochemical windows according to eqs 3−5.

Table 5. The Calculated Potentials (in V) of $[N_{1113}]^+[Tf_2N]^-$ Corresponding to the Redox Reactions Described in Figure 6[a]

	$V(R5)_{ox}$	$V(R10)_{red}$	$V(R11)_{red}$	ECW	Exp.[b]
vacuo	5.40	−2.82	−4.75	0.65	4.5−5.0[9]
PCM	7.00	−0.63	−2.52	4.48	
TDC	7.07		−2.57	4.50	
ONIOM	7.69		−2.62	5.07	

[a]The most negative reduction potentials are used to calculate the electrochemical windows according to eqs 3−5. [b]Measured for $[N_{6222}][Tf_2N]$, which is assumed to have electrochemical windows similar to that of $[N_{3111}][Tf_2N]$.

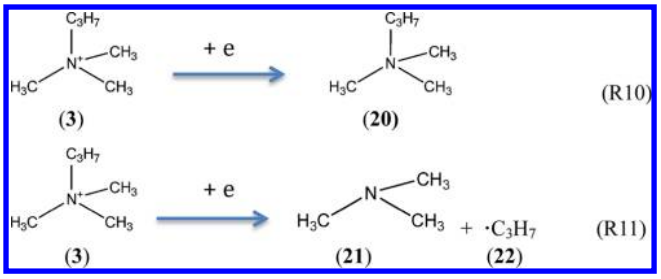

Figure 8. The reduction reactions of $[N_{3111}]^+$ cation used to calculate reduction potentials.

widely depending on the measurement conditions, our calculations are in general agreement with experiments. The calculations indicate that $[N_{1113}]^+[Tf_2N]^-$ systems show about 0.20, 0.03, or 0.46 V wider electrochemical windows than $[C_2MIM]^+[Tf_2N]^-$ at the PCM, TDC, or ONIOM level, respectively. Therefore, the broad trend is predicted that quaternary ammonium-based salts have wider electrochemical windows than imidazolium-based salts.[9] The reason for that can be understood by examining the solvation free energies. From Tables 2 and 6, it is noticed that the solvation free energies calculated at respective levels are similar for $[C_2MIM]^+$ and $[N_{3111}]^+$, while much stronger solvation is observed for the reduction product **9** than for the reduction product **21**. As a result, the wider electrochemical window for $[N_{3111}]^+[Tf2N]^-$ is a consequence of a stronger solvation effect of its reduction product. In molecule **9**, corresponding to reaction R2 shown in Figure 4, there are two lone-pairs of electrons (one σ plus one π long pair) around the nitrogen atoms involved in the bond breaking reactions, and hence the nitrogen is electron rich, resulting in strong solvation. On the other hand, in the reduction product of **21** shown in Figure 8, there is only one lone-pair of electrons, and hence weaker solvation is expected.

Pyrrolidinium (PYR) is a kind of cation with similar structure to quaternary ammonium (QA) except for the alkyl ring in the former. According to the CV experiments, PYR salts are more stable toward reduction than QA salts. It is of interest to computationally compare the electrochemical behavior for the two structurally similar systems. *N*,*N*-Propylmethylpyrrolidinium (PYR_{13}) (see Figure 1 for structure) was used for calculations. Similar to the reduction process of QA salts described in Figure 8, our calculations identified two possible reduction reactions involved of PYR cations, as illustrated in Figure 2S (Supporting Information). Electrochemical and spectroscopic measurements have shown evidence that, in the $[PYR_{13}]^+[Tf_2N]^-$ system, $[Tf_2N]^-$ anions probably undergo reductive decomposition,[21] as shown in eq R12. Accordingly, we also computationally examined this possibility. According to our calculations, the ammonium decomposing reduction (shown in Figure 2S, Supporting Information) is slightly more favorable than the reduction process R12. The reduction potentials corresponding to those two electrochemical processes are very close. Therefore, depending on the experimental conditions such as onset electrical current for potential limits and scanning rate of CV, both of the processes might occur.

$$N(SO_2CF_3)_2^- + e^- = \bullet NSO_2CF_3^- + SO_2CF_3^- \qquad (R12)$$

The calculated redox potentials and electrochemical widows are shown in Table 7. Although the predicted electrochemical window is smaller than experimental measurement, the trend is largely predicted that pyrrolidinium salts have wider electrochemical windows than their QA counterparts. Moreover, as quoted in Table 7, the experimental values, both measured with glass carbon electrode, expand in a wide range. Given the experimental uncertainty, our predicted trend seems more reliable, because it is close to the values of the QA analogues. Both the gas phase and PCM calculations suggest that the

Table 7. The Calculated Potentials (in V) of $[PYR_{13}]^+[Tf_2N]^-$ Corresponding to the Redution Reactions Shown in Figure 2S (Supporting Information)[a]

	$V(R5)_{ox}$	$V(R12)_{red}$	$V(R1)_{red}$	$V(R2)_{red}$	ECW	Exp.
vacuo	5.40	−0.36	−2.71	−4.45	0.95	5.5,[10 b] 4.2[34 c]
PCM	7.00	−2.11	−0.60	−2.27	4.73	

[a]$V_{red,1}$ and $V_{red,2}$ correspond to reactions R1 and R2, respectively, in Figure 2S (Supporting Information). [b]Electrochemical windows of $[(n\text{-}C_4H_9)(CH_3)PYR]^+[Tf_2N]^-$. [c]Electrochemical windows of $[(n\text{-}C_3H_9)(CH_3)PYR]^+[Tf_2N]^-$.

Table 6. Solvation Free Energies (in eV) Corresponding to the Redox Reactions R6 and R7 Described in Figure 6[a]

	$\Delta G(\mathbf{6})_s$	$\Delta G(\mathbf{14})_s$	$\Delta\Delta G_s^{R5}$	$\Delta G(\mathbf{3})_s$	$\Delta G(\mathbf{20})_s$	$\Delta\Delta G_s^{R10}$	$\Delta G(\mathbf{21,22})_s$	$\Delta\Delta G_{solv}^{R11}$
PCM	−1.59	0.01	1.60	−2.46	−0.28	2.18	−0.23	2.23
TDC	−1.75	−0.08	1.67	−2.24			−0.06	2.18

[a]$\Delta\Delta G_{solv}^{R6-R7}$ were calculated as the solvation free energy differences of the products and reactants as described in eqs 7 and 8.

dx.doi.org/10.1021/jp303915c | J. Phys. Chem. B 2012, 116, 11943−11952

reduction reaction corresponding to the bond breaking process is preferable over the other process. The PCM calculations indicate that $[PYR_{13}]^+[Tf_2N]^-$ is more resistant to reduction than $[N_{1113}]^+[Tf_2N]^-$. On the other hand, the solvation free energy changes upon reduction are comparable for the two systems. Consequently, the enhanced reduction stability for $[PYR_{13}]^+[Tf_2N]^-$ is intrinsically attributed to its electronic structure, which is reflected by its stronger reduction resistance according to gas phase calculations. Presumably, the alky ring in $[PYR_{13}]^+$ cation is more electron-giving than the alkyl chain in $[N_{113}]^+$, and hence the former cation is more stabilized.

Next, the electrochemical windows of phosphonium salts were examined. As in ammonium salts, two possible reduction reactions of cations were used for calculations, which are shown in the Supporting Information, Figure 3S. The estimated electrode potentials are summarized in Table 8. It is noticed

Table 8. The Calculated Potentials (in V) of $[P_{1113}][Tf_2N]$ Corresponding to the Reduction Reactions Shown in Figure 3S (Supporting Information)

	$V_{ox,1}$	$V_{red,1}$	$V_{red,2}$	ECW	Exp.
vacuo	5.40	−2.86	−4.12	1.38	5.2,[35] 6.3[11]
PCM	7.00	−0.75	−1.99	5.01	

that the experimental measurements vary widely even reported by the same research group. Our PCM calculations agree well with the latest reported measurement of 5.2 V. The general trend is predicted by PCM calculations that phosphonium based salts have a wider electrochemical window than ammonium salts.

4.3. The Predicted Trend. The calculated electrochemical windows are shown in Figure 9 against the experimental values

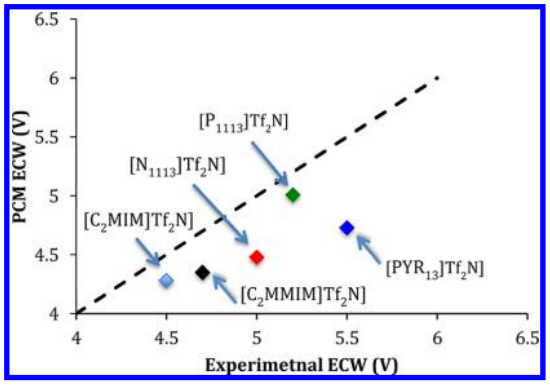

Figure 9. The plot of experimental ECW against the PCM calculations at the B2PLYPD level. A diagonal dashed line is used to guide eyes. The general trend is predicted that the ECWs increase in the order of imidazolium < ammonium < pyrrolidinium < phosphonium.

for the RTILs involved in this study. It is noted that the trend is predicted with the electrochemical windows increasing in the order of imidazolium < ammonium < pyrrolidinium < phosphonium, which is in agreement with experimental measurements. One exception is PYR cations, for which experimentally measured ECW lie in a wide range. In this respect, the position of the experimental value in the trend plot is uncertain. The predicted values by using the PCM model are largely in consistence with experimental measurements for a variety of RTIL systems.

5. CONCLUSIONS

Five types of RTILs showing a wide range of electrochemical windows were explored at a variety of theory levels including gas phase calculations, PCM, TDC, and ONIOM. The PCM, TDC, and ONIOM calculations show consistent results that agree fairly well with experimental measurements. We found that to predict the electrochemical windows of RTILs the PCM model represents a reasonable compromise between accuracy and efficiency. Special attention should be put in electronic and structural relaxations upon redox reaction. For imidazolium based RTILs, our calculations show that the cathodic potential limit is determined by the one-electron reduction reaction of the cations, in which bond scissions occur. The corresponding reduction product is stabilized because the extra electron upon reduction is accepted by the lone pair orbitals of nitrogen and the molecule remains aromatic due to 4 + 2 π-electrons. For ammonium, pyrrolidinium, and phosphonium salts, the most accessible reduction is involved in breaking one of the carbon−nitrogen or carbon−phosphorus bonds. For the structurally similar ammonium and pyrrolidinium salts, our calculations predicted a significantly wider electrochemical window for the later, which is in consistence with experimental observations.

■ ASSOCIATED CONTENT

Supporting Information

The redox reaction schemes for C_2MMIM, pyrrolidinium, and phosphonium systems, an example to illustrate how the redox potentials are calculated, and the complete list of authors for ref 19. This material is available free of charge via the Internet at http://pubs.acs.org.

■ AUTHOR INFORMATION

Corresponding Author

*E-mail: erb@lanl.gov.

Notes

The authors declare no competing financial interest.

■ ACKNOWLEDGMENTS

This work was funded by LRDR, Los Alamos National Laboratory. The Los Alamos National Laboratory is operated by Los Alamos National Security, LLC, for the National Nuclear Security Administration of the U.S. Department of Energy under Contract DE-AC5206NA25396. The authors thank Drs. William Ewing, Xiaoyan Chen, Edward Maginn, Bill Schneider, and Joan Brennecke for helpful discussion.

■ REFERENCES

(1) Rogers, R. D.; Seddo, K. R. *Science* **2003**, *302*, 792−793.
(2) (a) Sakaebe, H.; Matsumoto, H. *Electrochem. Commun.* **2003**, *5*, 594. (b) Nakagawa, N.; Izuchi, S.; Kuwana, K.; Nukuba, T.; Aihara, Y. *J. Electrochem. Soc.* **2003**, *150*, A695−A700. (c) Garcia, B.; Lavallee, S.; Perron, G.; Michot, C.; Armand, M. *Electrochim. Acta* **2004**, *49*, 4583. (d) Matsumoto, H.; Sakaebe, H.; Tatsumi, K.; Kikuta, M.; Ishiko, E.; Kono, M. *J. Power Sources* **2006**, *160*, 1308.
(3) Noda, A.; Susan, M. A. B. H.; Kubo, K.; Mitsushima, S.; Hayamizu, K.; Watanabe, M. *J. Phys. Chem. B* **2003**, *107*, 4024.
(4) (a) Papageorgiou, N.; Athanassov, Y.; Armand, M.; Bönhote, P.; Pettersson, H.; Azam, A.; Grätzel, M. *J. Electrochem. Soc.* **1996**, *143*, 3099. (b) Wang, P.; Zakeeruddin, S. M.; Moser, J.-E.; Grätzel, M. *J. Phys. Chem. B* **2003**, *107*, 13280. (c) Mikoshiba, S.; Murai, S.; Sumino, H.; Kado, T.; Kosugi, D.; Hayase, S. *Curr. Appl. Phys.* **2005**, *5*, 152.
(5) (a) Endres, F.; Abbott, A. P.; MacFarlane, D. R. *Electrodeposition from Ionic Liquids*; Wiley-VCH: Weinheim, Germany, 2008. (b) Binne-

mans, K. *Chem. Rev.* **2007**, *107*, 2592−2614. (c) Jagadeeswara Rao, C.; Venkatesan, K. A.; Nagarajan, K.; Srinivasan, T. G.; Vasudeva Rao, P. R. *J. Nucl. Mater.* **2011**, *408*, 25−29.
(6) (a) Noda, A.; Watanabe, M. *Electrochim. Acta* **2000**, *45*, 1265−1270. (b) Evans, E.; Klymenko, O. V.; Hardacre, C.; Seddon, K. R.; Compton, R. G. *J. Electroanal. Chem.* **2003**, *556*, 179−188.
(7) Seddon, K. R. In *The International George Papatheodorou Symposium: Proceedings*; Boghosian, S., Dracopoulos, V., Kontoyannis, C. G., Voyiatzis, G. A., Eds.; Institute of Chemical Engineering and High Temperature Chemical Processes: Patras, Greece, 1999; pp 131−135.
(8) Bonhôte, P.; Dias, A.-P.; Papageorgiou, N.; Kalyanasundaram, K.; Gra1tzel, M. *Inorg. Chem.* **1996**, *35*, 1168−1178.
(9) (a) McFarlane, D. R.; Sun, J.; Golding, J.; Meakin, P.; Forsyth, M. *J. Electrochim. Acta* **2000**, *45*, 1271−1278. (b) Rogers, E. I.; Sljukic, B; Hardacre, C; Compton, R. G. *Chem. Eng. Data* **2009**, *54*, 2049−2053. (c) Matsumoto, H.; Yanagida, M.; Tanimoto, K.; Nomura, M.; Kitagawa, Y.; Miyazaki, Y. *Chem. Lett.* **2000**, 922−923. (d) MacFarlane, D. R.; Meakin, P.; Sun, J.; Amini, N.; Forsyth, M. *J. Phys. Chem. B* **1999**, *103*, 4164−4170.
(10) Sun, J.; Forsyth, M.; MacFarlane, D. R. *J. Phys. Chem. B* **1998**, *102*, 8858−8864.
(11) Tsunashima, K.; Sugiya, M. *Electrochem. Commun.* **2007**, *9*, 2353−2358.
(12) (a) Suarez, P. A. Z.; Selbach, V. M.; Dullius, J. E. L.; Einloft, S.; Piatnicki, C. M. S.; Azambuja, D. S.; Souza, R. F. de; Dupont, J. *Electrochim. Acta* **1997**, *42*, 2533−2535. (b) Fuller, J.; Carlin, R. T.; Osteryoung, R. A. *J. Electrochem. Soc.* **1997**, *144*, 3881−3886. (c) Nanjundiah, C.; McDevitt, S. F.; Koch, V. R. *J. Electrochem. Soc.* **1997**, *144*, 3392−3397. (d) Koch, V. R.; Dominey, L. A.; Nanjundiah, C.; Ondrechen, M. J. *J. Electrochem. Soc.* **1996**, *143*, 798−803.
(13) (a) Arduengo, A. J.; Harlow, R. L.; Kline, M. *J. Am. Chem. Soc.* **1991**, *113*, 361. (b) Arduengo, A. J.; Dias, H. V. R; Harlow, R. L.; Kline, M. *J. Am. Chem. Soc.* **1992**, *114*, 5530. (c) Kuhn, H.; Bohnen, H.; Kreutzberg, J.; Bläser, D.; Boese, R. *Chem. Commun.* **1993**, 1136−1137.
(14) Kroon, M. C.; Buijs, W.; Peters, C. J.; Witkamp, G.-J. *Green Chem.* **2006**, *8*, 241−245.
(15) Maeshima, H.; Moriwake, H.; Kuwabara, A.; Fisher, C. A. J. *J. Electrochem. Soc.* **2010**, *157*, A696−A701.
(16) Ong, S. P.; Andreussi, O.; Wu, Y.; Marzari, N.; Ceder, G. *Chem. Mater.* **2011**, *23*, 2979−2986.
(17) Ong, S. P.; Ceder, G. *Electrochim. Acta* **2010**, *55*, 3804−3811.
(18) McQuarrie, D. A.; Simon, J. D. *Molecular Thermodynamics*; University Science Books: California, 1999.
(19) Frisch, M. J.; et al. *Gaussian 09*, revision A.1; Gaussian, Inc.: Wallingford, CT, 2009.
(20) Marenich, A. V.; Cramer, C. J.; Truhlar, D. G. *J. Phys. Chem. B* **2009**, *113*, 6378−6396.
(21) Howlett, P. C.; Izgorodina, E. I.; Forsyth, M.; MacFarlane, D. R. *Z. Phys. Chem.* **2006**, *220*, 1483−1498.
(22) Weingartner, H. *Z. Phys Chem.* **2006**, *220*, 1395−1405.
(23) Roy, L. E.; Batista, E. R.; Hay, P. J. *Inorg. Chem.* **2008**, *47*, 9228−9237.
(24) Vreven, T.; Byun, K. S.; Komáromi, I.; Dapprich, S.; Montgomery, J. A.; Morokuma, K.; Frisch, M. J. *J. Chem. Theory Comput.* **2006**, *2*, 815−826.
(25) (a) Pohorille, A.; Jarzynski, C.; Chipot, C. *J. Phys. Chem. B* **2010**, *114*, 10235−10253. (b) Christ, C. D.; Mark, A. E.; van Gunsteren, W. F. *J. Comput. Chem.* **2010**, *31*, 1569−1582.
(26) Bennett, C. H. *J. Comput. Phys.* **1976**, *22*, 245.
(27) Klähn, M.; Seduraman, A.; Wu, P. *J. Phys. Chem. B* **2011**, *115*, 8231−8241.
(28) Grimme, S. *J. Chem. Phys.* **2006**, *124*, 034108.
(29) Van der Spoel, D.; Lindahl, E.; Hess, B.; Groenhof, G.; Mark, A. E.; Berendsen, H. J. C. J. *J. Comput. Chem.* **2005**, *26*, 1701−1718.
(30) (a) Lopes, J. N. C.; Pádua, A. A. H. *J. Phys. Chem. B* **2004**, *108*, 16893−16898. (b) Lopes, J. N. C.; Pádua, A. A. H. *J. Phys. Chem. B* **2006**, *110*, 19586−19592.
(31) McEwen, A. B.; Ngo, H. L.; LeCompte, K.; Goldman, J. L. *J. Electrochem. Soc.* **1999**, *146*, 1687.
(32) Borodin, O. *J. Phys. Chem. B* **2009**, *113*, 11463−11478.
(33) Kim, J; Shreeve, J. M. *Org. Biomol. Chem.* **2004**, *2*, 2728−2734.
(34) Pringle, J. M.; Golding, J.; Baranyani, K.; Forsyth, C. M.; Deacon, G. B.; Scott, J. L.; MacFarlane, D. R. *New J. Chem.* **2003**, *27*, 1504.
(35) Tsunashima, K.; Ono, Y.; Sugiya, M. *Electrochim. Acta* **2011**, *56*, 4351−4355.